A global picture of the first abrupt climatic event occurring during the last glacial inception

E. Capron,[1,2] A. Landais,[1] J. Chappellaz,[3] D. Buiron,[3] H. Fischer,[4,5] S. J. Johnsen,[6] J. Jouzel,[1] M. Leuenberger,[4] V. Masson-Delmotte,[1] and T. F. Stocker[4]

Received 6 June 2012; revised 29 June 2012; accepted 29 June 2012; published 4 August 2012.

[1] The orbital-scale transition from the last interglacial to glacial climate corresponds to the progressive organization of global millennial-scale climate variability. Here, we investigate the structure and the global fingerprint of the first warming event occurring during the last glacial inception, the Greenland InterStadial 25 (GIS 25). Using centennial to decadal-resolution measurements of $\delta^{18}O$ and δD in the ice together with $\delta^{15}N$, $\delta^{18}O_2$ and CH_4 in the trapped air, we show that GIS 25 does not coincide with large environmental changes at lower latitudes. Such an equivocal fingerprint questions whether GIS 25 is simply a smaller amplitude version of later rapid events or whether it reflects a more regional northern hemisphere origin for the initiation of the millennial-scale climatic variability. After this ambiguous first rapid event, the onset of the global millennial-scale variability -characteristic of the last glacial period- occurs as a short (300 years) event ending GIS 25. **Citation:** Capron, E., A. Landais, J. Chappellaz, D. Buiron, H. Fischer, S. J. Johnsen, J. Jouzel, M. Leuenberger, V. Masson-Delmotte, and T. F. Stocker (2012), A global picture of the first abrupt climatic event occurring during the last glacial inception, *Geophys. Res. Lett.*, *39*, L15703, doi:10.1029/2012GL052656.

1. Introduction

[2] Major global climate reorganisations take place at the transition between relatively short and stable interglacial periods, and relatively long and variable glacial periods. While the role of orbital forcing on changes in the latitudinal and seasonal distribution of insolation is recognized to be an important driver for glacial inceptions [e.g., *Berger*, 1988], open questions remain regarding the onset, cause and role of millennial variability within such transitions. Fully understanding and simulating these rapid changes are critical challenges as they indicate an important instability of the Earth climate and thus, may have important implications for predictions of future climate and constraining the boundary conditions required to initiate rapid climate change.

[3] The transition between the Last Interglacial (hereafter Marine Isotopic Stage 5.5, ~129–116 thousand years before present (ka)) into the first stage of the last glacial period (MIS 5.4, ~116–105 ka) is the only glacial inception recorded in Greenlandic ice cores [*NorthGRIP Community Members*, 2004]. It is generally accepted that this transition is characterized by progressive ice sheet growth in response to the climatic amplification of astronomical forcing, through, e.g., the snow/ice albedo feedback [e.g., *Khodri et al.*, 2001; *Wang and Mysak*, 2002; *Tziperman et al.*, 2006; *Jochum et al.*, 2012]. At least one quarter of the ice sheet volume during full glacial conditions is reached at MIS 5.4 [*Bintanja et al.*, 2005; *Thompson and Goldstein*, 2005] (Figure 1). This transition is associated with a small millennial-scale warming event first identified in Northern Atlantic marine records [*Chapman and Shackleton*, 1999; *Oppo et al.*, 2006] and labelled Dansgaard-Oeschger (DO) event 25 in the North-GRIP $\delta^{18}O_{ice}$ record [*NorthGRIP Community Members*, 2004].

[4] DO events are a classical feature of the last glacial period [*NorthGRIP Community Members*, 2004]. A DO event is classically described as an abrupt warming reaching 8–16°C within decades in Greenland [*Huber et al.*, 2006; *Landais et al.*, 2006], leading to a transient warm phase (GIS for Greenland Interstadial) followed by a slower cooling and generally culminating in a rapid return to the cold stadial state (GS for Greenland Stadial) (Figure 1). DO events have worldwide reverberations captured by oceanic and continental records [*Voelker et al.*, 2002], changes in atmospheric composition [*Chappellaz et al.*, 1993], and their one-to-one Antarctic counterparts [*EPICA Community Members*, 2006; *Capron et al.*, 2010a] confirm the bipolar seesaw mechanism predicted in a simple model [*Stocker and Johnsen*, 2003]. They are commonly thought to be linked with significant shifts in the strength of the Atlantic Meridional Overturning Circulation (AMOC), related to glacial ice sheet meltwater discharge into the North Atlantic Ocean [*Broecker*, 1998; *Stocker*, 2000]. However, modelling the glacial climatic millennial-scale variability related to changes in the AMOC is still challenging (*Kageyama et al.* [2010] for a review) and mechanisms or threshold-crossing events in the Tropics or the Southern Hemisphere for triggering abrupt climatic events are not ruled out [*Cane*, 1998; *Knorr and Lohmann*, 2003]. A crucial problem is thus to document the triggering and the structure of early DO events during the glacial inception compared to classical DO events of MIS 3.

[1]Laboratoire des Sciences du Climat et de l'Environnement, Institut Pierre-Simon Laplace, CEA-CNRS-UVSQ, Gif-sur-Yvette, France.
[2]British Antarctic Survey, NERC, Cambridge, UK.
[3]Laboratoire de Glaciologie et Géophysique de l'Environnement, CNRS-UJF, St-Martin-d'Hères, France.
[4]Climate and Environmental Physics, Physics Institute and Oeschger Centre for Climate Change Research, University of Bern, Bern, Switzerland.
[5]Alfred Wegener Institute for Polar and Marine Research, Bremerhaven, Germany.
[6]Department of Geophysics, University of Copenhagen, Copenhagen, Denmark.

Corresponding author: E. Capron, British Antarctic Survey, NERC, High Cross, Madingley Road, Cambridge CB4 3BE, UK. (ecap@bas.ac.uk)

0094-8276/12/2012GL052656

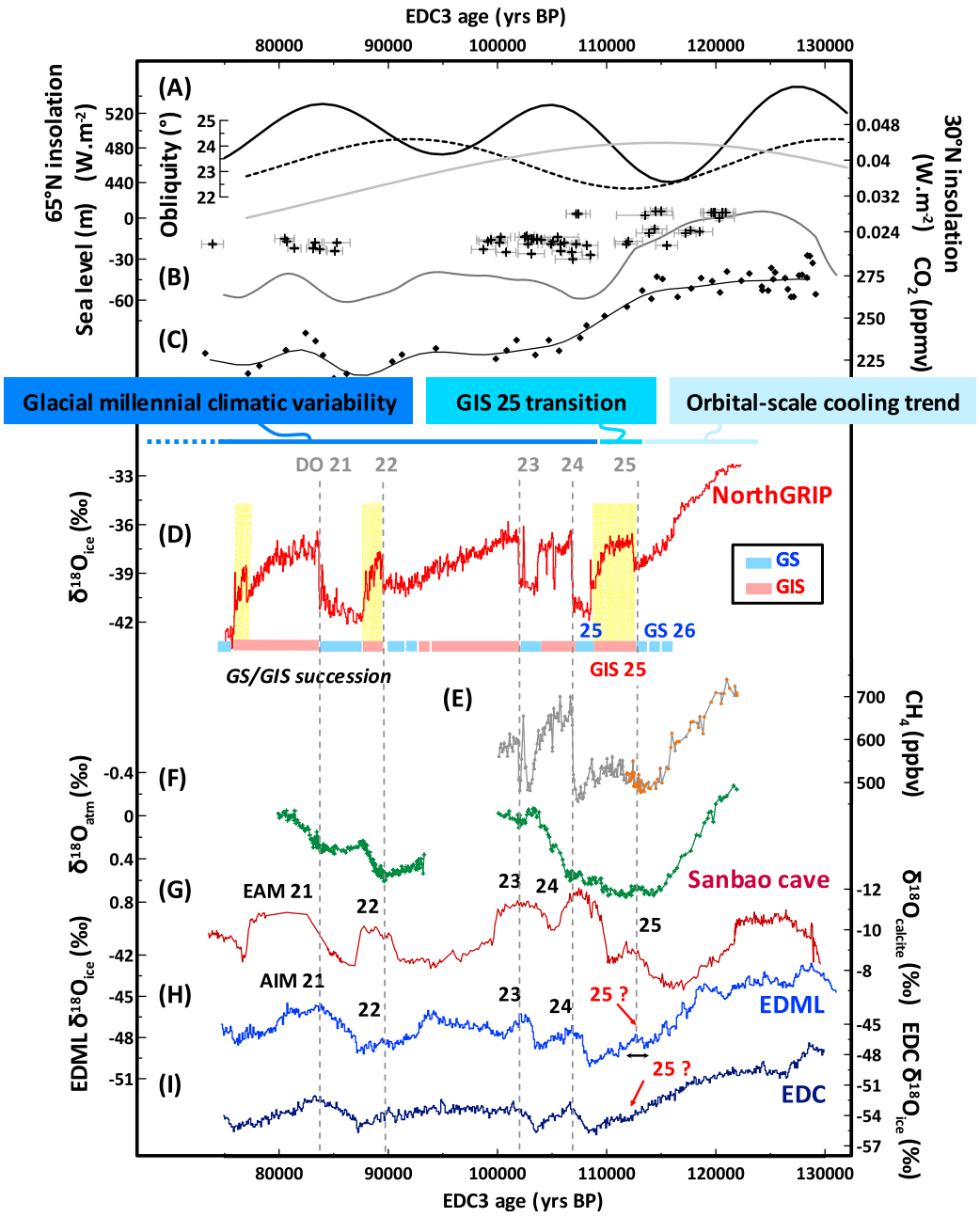

Figure 1. (a) 65°N insolation (black), 30°N insolation (grey) and obliquity (dashed black) [*Laskar et al.*, 2004]. (b) Sea level relative to present, reconstructions from *Bintanja et al.* [2005] (grey curve) and *Thompson and Goldstein* [2005] (black crosses with associated uncertainties). (c) CO_2 data [*Lüthi et al.*, 2008], smoothed curve (black) produced from a five-point binomial filter using 1200-yr resampled data. (d) NorthGRIP $\delta^{18}O_{ice}$ [*NorthGRIP Community Members*, 2004]. GIS beginning is marked by an abrupt warming referred to as DO. Yellow boxes indicate rebound-type structures: GIS 22, GIS 25 and the rapid event ending GIS 21 [*Capron et al.*, 2010a]. (e) NorthGRIP CH_4 grey triangle: *Capron et al.* [2010b]; this study: red triangle). (f) NorthGRIP $\delta^{18}O_{atm}$ [*Landais et al.*, 2010]. (g) $\delta^{18}O_{calcite}$ of Sanbao Cave speleothems [*Wang et al.*, 2008]. (h) EDML $\delta^{18}O_{ice}$ [*Stenni et al.*, 2010]. Antarctic Isotopic Maximum events are indicated (AIM). (i) EDC $\delta^{18}O_{ice}$. *Jouzel et al.* [2007] and *Stenni et al.* [2010] have suggested that an Antarctic counterpart of DO 25, named AIM 25, was visible in $\delta^{18}O_{ice}$ profiles from the EPICA ice cores: the millennial-scale event identified as AIM 25 is indicated for each record by the red arrow. The associated question marks illustrate that such identification remains equivocal. Except for the Sanbao $\delta^{18}O_{calcite}$ record, the orbital parameters, and the sea level reconstruction from *Thompson and Goldstein* [2005], records are synchronised on the EDC3 timescale [*Parrenin et al.*, 2007; *Capron et al.*, 2010b]. Dashed light pink lines indicate rapid event onsets. The black arrow indicates the temporal uncertainty linked to the timescale synchronisation at the onset of GIS 25. The horizontal bar indicates the GIS/GS succession and dots indicate the ambiguity that remains on defining the start of GS 26 and GS 23.

[5] Up to now, the only ice core from Greenland able to depict the continuous sequence of the last glacial inception is the NorthGRIP ice core, providing a wealth of climatic and environmental proxies, and an exceptionally high resolution over this sequence (annual layer thickness of the order of 1 cm [*NorthGRIP Community Members*, 2004]). At NorthGRIP, the long-term cooling trend between 123 ka and 116 ka due to decreasing obliquity and precession-forced insolation is interrupted at 116 ka by GIS 25 which lasts 4700 ± 140 years (Figure 2). This climatic sequence is very similar to the one observed over the long interstadials of MIS 5, GIS 21 and GIS 23. They display a short-lived abrupt warming called "rebound" event following a progressive cooling phase [*Capron et al.*, 2010a]. Thus, DO 25 can be viewed as the "rebound" event ending MIS 5.5. The presence of such characteristic structures associated with rebound-type events demonstrates that the millennial scale climatic variability in Greenland is more complex than the GS/GIS succession classically described (Figure 1).

[6] Previous studies have already pointed out the peculiarities of DO 25, with characteristics different from classical DO events [*Chapman and Shackleton*, 1999; *Oppo et al.*, 2006; *Landais et al.*, 2006; *Sanchez-Goñi et al.*, 2002]. Still, high-resolution data do not show the precise North Atlantic sequence of events over the last glacial inception and how this is linked to climatic and environmental changes in the lower latitudes. Here we employ the NorthGRIP record to report a detailed picture of the onset of the rapid climatic variability in Greenland and in the lower latitudes based on

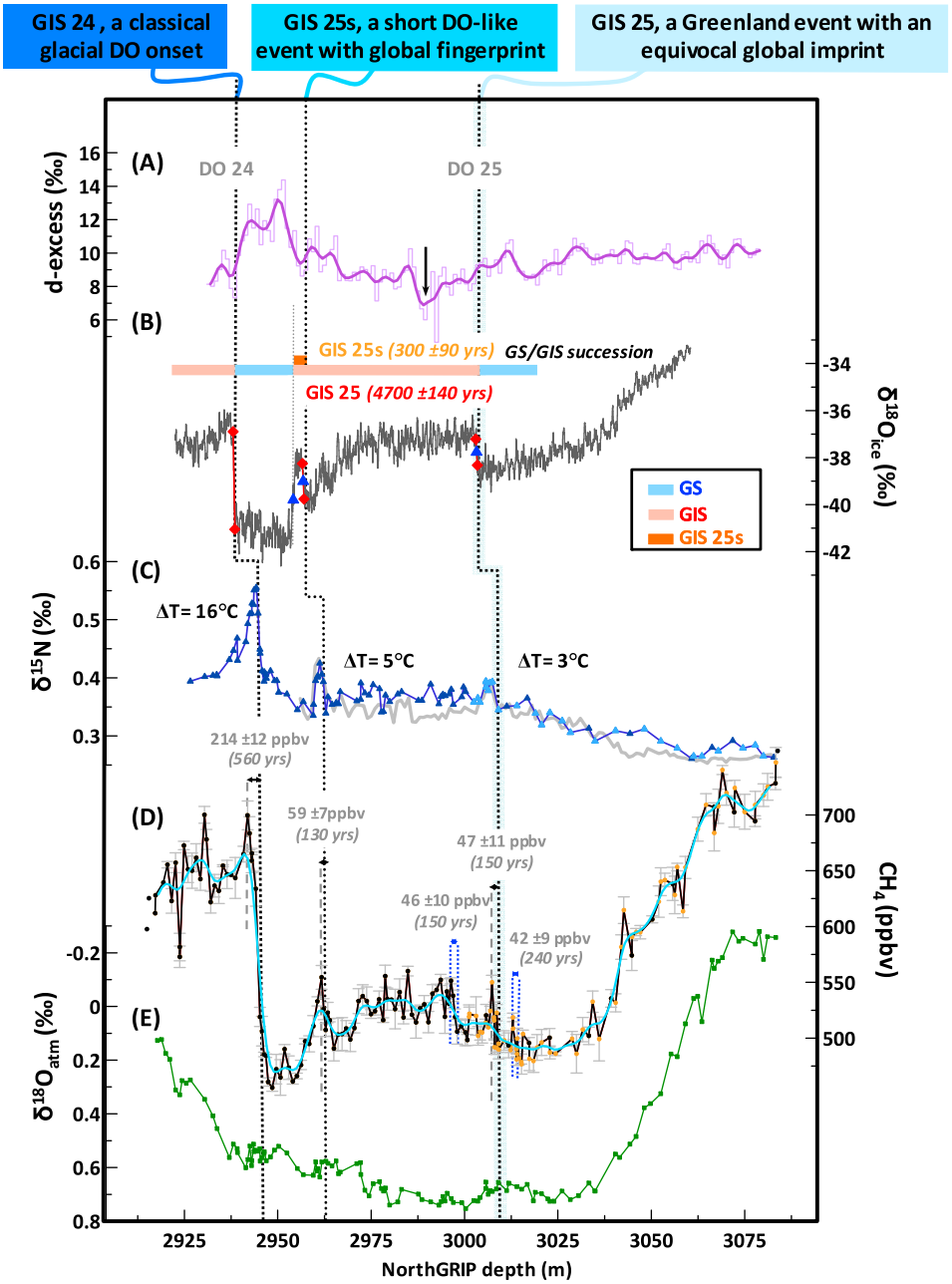

Figure 2

Table 1. New Measurements Over DO 25 Event

Number of New Data Points		Method	Uncertainty	Temporal Resolution[a]	Reference
$\delta^{18}O_{ice}$	3081	*Epstein* [1953]	0.07‰	99.3–123 kyr: 6 yr	This study
δD	267	*Vaughn et al.* [1998] and *Epstein* [1953]	δD: 0.5‰ d-excess: 0.7‰	99.3–12 kyr: 70 yr	δD: This study $\delta^{18}O_{ice}$: *Stenni et al.* [2010]
$\delta^{15}N$	56[b]	*Landais et al.* [2004a]	0.006‰	111–123 ka: 100 yr 114–117 ka: 110 yr	*Landais et al.* [2006] and This study
CH_4	65	*Chappellaz et al.* [1993]	8 ppbv	111–123 ka: 100 yr 114–118 ka: 70 yr	*Capron et al.* [2010b] and This study

[a]The temporal resolution is deduced from the age/depth relationship of the NorthGRIP glaciological timescale [*NorthGRIP Community Members*, 2004]. The overall temporal resolution is given after combining our new data with published measurements.
[b]Twenty-eight duplicate depth levels.

new high-resolution (centennial to sub-decadal) profiles of a wide range of parameters measured on both ice and air trapped in ice (Figure 2 and Table 1).

2. Data and Methods

[7] New air isotopes ($\delta^{15}N$ of N_2, $\delta^{18}O$ of O_2) and methane concentration measurements were performed on the trapped air of the NorthGRIP ice core. A high resolution profile of $\delta^{18}O$ of the ice ($\delta^{18}O_{ice}$) was obtained over the last glacial inception, along with a δD profile which in combination yields the deuterium excess (d-excess = $\delta D - 8 \times \delta^{18}O$ [*Dansgaard*, 1964]). See Table 1 and Appendix A for details.

[8] Estimating the magnitude of the Greenland temperature shift at the onset of GIS 25 is not straightforward since $\delta^{18}O_{ice}$ is affected by precipitation seasonality and/or shifts in moisture sources [e.g., *Masson-Delmotte et al.*, 2005]. The combined use of positive anomalies of $\delta^{15}N$ together with the modelling of physical processes occurring in the firn (e.g., densification, heat diffusion [*Goujon et al.*, 2003]) provides a quantitative estimate of the amplitude of rapid surface temperature increases [e.g., *Severinghaus et al.*, 1998; *Landais et al.*, 2004a, 2006; *Huber et al.*, 2006]. Here, using a firnification and heat diffusion model [*Goujon et al.*, 2003], it is possible to reproduce the $\delta^{15}N$ evolution by adjusting the prescribed surface temperature scenario that is originally based on water isotopic records. The associated uncertainty of 2.5°C is estimated from sensitivity experiments performed using varying surface temperature scenarios as model inputs [*Landais et al.*, 2004a].

3. Results

[9] We first present new high-resolution $\delta^{18}O_{ice}$ measurements covering the glacial inception between 108 and 123 ka (Figure 2 and Table 1). Two abrupt increases of $\delta^{18}O_{ice}$ are objectively identified in this time interval and quantified using the RAMPFIT software [*Mudelsee*, 2000]. This weighted least-squares method estimates the level of the $\delta^{18}O_{ice}$ for stadial and interstadial conditions, a linear trend between the change points, and a measure of the uncertainty of these estimated change points based on a set of 400 bootstrap simulations for each abrupt event. The onset of GIS 25 is characterized by a $\delta^{18}O_{ice}$ increase of 1.12 ± 0.05 ‰ and the end of GIS 25 is punctuated by a second abrupt $\delta^{18}O_{ice}$ increase of 1.51 ± 0.04 ‰. This sub-event is referred later as GIS 25 s. These magnitudes are significantly reduced in comparison to subsequent GIS onsets (Figure 1). Note that

Figure 2. NorthGRIP high-resolution climatic records over GIS 25. Our NorthGRIP timescale tuned on the EDC3 timescale [*Capron et al.*, 2010b; *Parrenin et al.*, 2007] lacks of glaciological constraints, which can lead to inconsistency when calculating the duration of short events like GIS 25 s. We thus present the high-resolution profiles on a depth scale. Temporal information and calculation for the duration of short events are deduced using the glaciological thinning function obtained at the bottom of the NorthGRIP ice core by *NorthGRIP Community Members* [2004]. Note that climatic events are recorded deeper in the gas than in the ice since air is isolated from the atmosphere at the bottom of the firn column. Black dotted lines indicate the onset of GIS 25, 25 s and 24 determined with the RAMPFIT software [*Mudelsee*, 2000] in the $\delta^{18}O_{ice}$ record and the correspondence in the gas phase based on the $\delta^{15}N$ profile. (a) d-excess (raw data, thin line; smoothed curve (thick line) produced from a three-point binomial filter using one meter- resampled data, the black arrow marks the start of the d-excess increase in the course of GIS 25. (b) $\delta^{18}O_{ice}$. Red diamonds represent $\delta^{18}O_{ice}$ amplitude determined with RAMPFIT software [*Mudelsee*, 2000]. GIS 25 and GIS 25 s durations are given based on temporal values of the mid-slopes of the ramps estimated by the RAMPFIT software at the onset of GIS 25 (DO 25), GIS 25 s and the mid-slope of the ramp determined for the abrupt transition toward GS 25 (blue triangle). Note that the GIS 25 duration includes GIS 25 s. (c) $\delta^{15}N$ measurements (dark blue triangle: data from *Landais et al.* [2006], light triangle: this study). Modelled $\delta^{15}N$ (grey line) is superimposed and deduced from a heat diffusion model [*Goujon et al.*, 2003]. (d) CH_4: published (33) (black), this study (orange). Measurement uncertainties (2σ) are indicated (grey). The amplitude of CH_4 increase parallel to the rapid $\delta^{15}N$ increase is indicated for DO 24, DO 25 and GIS 25 s onset with the associated duration of the increase. The duration is calculated as the time-interval between the onset of the CH_4 increase corresponding to the onset of the $\delta^{15}N$ rapid increase (black dotted line) and the end of the CH_4 rapid increase, taken as the relative CH_4 maximum (grey dashed line). Blue dotted lines indicate two significant rapid CH_4 increases occurring during GS 26 and GIS 25, the associated amplitude and the duration of the CH_4 increase are given. The turquoise curve is the result of a five-point smoothing after a meter-resampling on the original dataset. Despite the smoothing, the onsets of GIS 24 and GIS 25 s are associated with a significant rapid increase in CH_4. In contrast, the CH_4 profile shows a slow increase beginning during GS 26. (e) $\delta^{18}O_{atm}$ [*Landais et al.*, 2010].

while the location of GIS 25 close to bedrock (80 m) favours a strong influence of ice diffusion, this will only dampen $\delta^{18}O_{ice}$ high frequency variability [*Johnsen et al.*, 2000] and the rate of abrupt variations but this should not affect the magnitude of abrupt stepwise $\delta^{18}O_{ice}$ shifts.

[10] Our new high resolution $\delta^{15}N$ profile reveals an increase of 0.044‰ at GIS 25 onset. Using the firn densification model from *Goujon et al.* [2003], the best fit between measured and modelled $\delta^{15}N$ is obtained for a warming of 3 ± 2.5°C. The warming at the onset of GIS 25 occurs in 180 years and is three to up to five times smaller than for the subsequent abrupt events [e.g., *Landais et al.*, 2006]. We also show that GIS 25 is then terminated by a previously undocumented short warm event, GIS 25 s, lasting 300 ± 90 years with a amplitude of 5 ± 2.5°C (Figure 2). Note, that our detailed $\delta^{15}N$ and $\delta^{18}O_{atm}$ (proxy for low frequency biospheric and hydrological changes [*Landais et al.*, 2010; *Severinghaus et al.*, 2009]) does not show any significant changes at the same depth as the shift in $\delta^{18}O_{ice}$ marking DO 25 onset [*Landais et al.*, 2006]. This confirms that DO 25 is of climatic origin and does not result from stratigraphic disturbances [e.g., *Landais et al.*, 2004b; *Fuchs and Leuenberger*, 1996]. The $\delta^{15}N$ increase associated with GIS 25 s onset occurs at the same depth as a sharp methane peak of 59 ± 7 ppbv. Such synchroneity between $\delta^{15}N$ and CH_4 is systematic during subsequent DO events [e.g., *Huber et al.*, 2006] and classically interpreted as reflecting changing emissions from tropical and boreal wetlands in phase with Greenland temperature [*Chappellaz et al.*, 1993].

[11] In contrast, no clear CH_4 signal is associated with the $\delta^{15}N$ peak marking DO 25. Indeed, a 47 ± 11 ppbv CH_4 increase is concurrent to GIS 25 onset, an amplitude also encountered during two other CH_4 peaks identified during GS 26 and GIS 25 when no significant Greenland temperature change is registered. This contrasts with the CH_4 shifts between 80 to 200 ppbv that are associated with the glacial DO events [*Chappellaz et al.*, 1993] (Figure 2). Such a small CH_4 increase could result from the fact that the temperature rise at the onset of GIS 25 is also significantly smaller than the one observed for the subsequent rapid events as the temperature sensitivity of the CH_4 change at the onset of GIS 25 is in the observed range of later rapid events. But the fact that there are other CH_4 signals of similar strength without a corresponding temperature shift points to an additional temperature-independent driver of CH_4 changes during glacial inception. The reduced CH_4 change at the onset of GIS 25 compared to later rapid events indicates that neither boreal nor tropical CH_4 sources significantly responded to this abrupt warming. It is also possibly related to the fact that GIS 25 occurs at a time corresponding to a relative minimum in the 30°N summer insolation, damping the effect of changes in the hydrological cycle on CH_4 sources (Figure 1). Indeed, it has been previously pointed out that this precession-forced parameter was modulating the amplitude of DO imprints in CH_4 [*Brook et al.*, 1996; *Flückiger et al.*, 2004].

[12] The isotopic composition of atmospheric oxygen ($\delta^{18}O_{atm}$) is also an integrated signal incorporating contributions from low latitudes. $\delta^{18}O_{atm}$ records have revealed smoothed millennial-scale variations marked by a systematic increase over GS and a decrease over GIS (Figure 1) [*Severinghaus et al.*, 2009). After comparison with the $\delta^{18}O$ of calcite ($\delta^{18}O_{calcite}$) from Chinese speleothems [*Wang et al.*, 2008], those millennial-scale variations were suggested to reflect changes in the vegetation distribution and in the low latitude hydrological cycle over abrupt events related to the monsoon activity, itself influenced by shifts in the InterTropical Convergence Zone [*Landais et al.*, 2010; *Severinghaus et al.*, 2009]. Although the $\delta^{18}O_{atm}$ variations are of smaller amplitude, we can distinguish an inverse pattern over the glacial inception. Indeed, while $\delta^{18}O_{atm}$ is increasing over the later GS, it decreases slightly by 0.06 ‰ during GS 26 in parallel to the CH_4 trend. Also, $\delta^{18}O_{atm}$ increases by 0.07 ‰ during GIS 25 (Figure 2) while other interstadials are associated with a decrease of $\delta^{18}O_{atm}$. This result suggests that there is not a simple coupling between high-latitude temperature and ITCZ shifts during abrupt climatic events that holds for all time periods.

[13] Deuterium excess in polar ice is used as a tracer for climatic conditions prevailing in the oceanic moisture source regions. Over DO 25, a negative 1 ‰ excursion is identified concurrent to GIS 25 s (Figure 2) interrupting a long-term d-excess increase that starts in the course of GIS 25. An anti-phase behaviour is also observed for the sequence of GS 25-GIS 24 with a clear decrease of d-excess by 4 ‰ corresponding to DO 24. This is consistent with the $\delta^{18}O_{ice}$/d-excess antiphase behaviour between 12 and 100 ka observed in Greenlandic ice cores, interpreted to reflect a significant warming of the Greenland moisture source region, induced by southward source shifts at each GS onset [e.g., *Masson-Delmotte et al.*, 2005]. The existence of such an antiphase behaviour between $\delta^{18}O_{ice}$/d-excess at the onset of GIS 25 remains equivocal. Indeed, a rapid 1‰-drop occurs simultaneously to the onset of GIS 25 but this is embedded in a long-term decrease of d-excess which already starts over GS 26. Thus, it seems unlikely that the onset of GIS 25 is associated with major modifications of the North Atlantic hydrological cycle. Also, the d-excess trend changes in the course of GIS 25 when d-excess starts increasing without any corresponding variation in the $\delta^{18}O_{ice}$ (Figure 2). Slow changes in the location of the moisture source likely occurred during the glacial inception because of decreasing local insolation, but the coupled behaviour between abrupt shifts in Greenland temperature and moisture source location is likely to have started only at GIS 25 s, simultaneously with the clear coupling between Greenland abrupt warming and CH_4 increase.

4. Discussion and Conclusions

[14] Altogether, the comparison of $\delta^{18}O_{atm}$, CH_4, d-excess, $\delta^{15}N$ and $\delta^{18}O_{ice}$ on the same ice core suggests that DO 25 is less pronounced than later DO events and that the coupling between low and high latitudes over DO 25 is different than for subsequent events.

[15] First, the weak effect of DO 25 on the low latitude hydrology could be explained by an asymmetrical polar ice sheet growth during the glacial inception. Indeed, moderate warmth and a strong AMOC during the glacial inception have been demonstrated, and have been suggested to act as a strong positive feedback to fuel northern ice-sheet growth [*McManus et al.*, 2002; *Guihou et al.*, 2010, 2011; *Khodri et al.*, 2001; *Wang and Mysak*, 2002] by providing heat and moisture to the high latitudes during winter [*Denton et al.*, 2005]. Since the thermal inertia of the Southern Ocean delays the Antarctic cooling, an interhemispheric thermal asymmetry could be created that would shift the

ITCZ southward [*Chiang and Bitz*, 2005]. We speculate that for such extreme southward positions of the ITCZ, its sensitivity to DO changes in the North Atlantic is muted, while atypically strong rainfall in the southern low latitude regions would prevail over the glacial inception. The $\delta^{18}O_{calcite}$ from Sanbao cave exhibits an event, the East Asian Monsoon event 25 (EAM 25), during the glacial inception that is significantly smaller than the subsequent EAM [*Wang et al.*, 2008] (Figure 1). Unfortunately, dating uncertainties preclude a precise discussion of the sequence of events between the speleothem and ice core records, so we cannot distinguish whether EAM 25 is related to Greenland in the classical DO fashion. Considering those dating issues, one should also be cautious in interpreting the small isotopic event recently identified in the benthic $\delta^{18}O$ record from the China Sea and interpreted as a response to ice volume variations to the Antarctic counterpart of DO 25 [*Caballero-Gill et al.*, 2012].

[16] Additionally, in contrast with the subsequent GS, the identification of an Antarctic counterpart to DO 25 is still ambiguous (Figure 1) as a precise synchronization of Greenland and Antarctic ice cores through CH_4 records is complicated over this time interval [*Capron et al.*, 2010b]. Indeed, the short NorthGRIP CH_4 peaks cannot be recorded in the current Antarctic ice cores because of the slower enclosure process [*Spahni et al.*, 2003]. In addition, the smoothed CH_4 increase observed when considering a low-pass filtered CH_4 curve over GS 26 and GIS 25 precludes the precise identification of a CH_4 stratigraphic marker between NorthGRIP and Antarctic ice cores (Figure 2). Finally, the high-frequency Antarctic $\delta^{18}O_{ice}$ records of the glacial inception show strong differences among different ice cores: the EPICA Dome C (EDC) $\delta^{18}O_{ice}$ profile displays only a small "inflection" interrupting the regular decrease, while the EPICA Dronning Maud Land (EDML) $\delta^{18}O_{ice}$ profile exhibits several centennial-scale variations (Figure 1) [*Stenni et al.*, 2010; *Jouzel et al.*, 2007]. Consequently, we cannot firmly assess the existence of an Antarctic counterpart to DO 25.

[17] To summarize, our results indicate that the first abrupt warming event, GIS 25, over the glacial inception is of significantly smaller amplitude (3 ± 2.5°C) than subsequent events (from 8 to 16°C [*Huber et al.*, 2006; *Landais et al.*, 2006]). We show that GIS 25 does not have the clear global fingerprint as demonstrated for later rapid events. The onset of the classical millennial-scale variability with a clear, broad spatial signature occurs only at the end of GIS 25, during the brief GIS 25 s event. Since GIS 25 warming is of reduced amplitude compared to the subsequent rapid events, one could expect that the global response to this event should also be small, as observed in CH_4 and d-excess records. This interpretation implies that this first abrupt event is likely driven by the same physical processes as the later events. Alternatively, based on CH_4 and d-excess patterns, together with the anomalous relationship observed between Greenland temperature and $\delta^{18}O_{atm}$ data, we speculate that a different coupling between the high and low latitudes is at play during GIS 25 compared to later rapid events, and that GIS 25 represents a regional feature in the Greenland/North Atlantic region that ends MIS 5.5. The first Greenlandic warming event is likely neither associated with significant iceberg discharge [*Chapman and Shackleton*, 1999; *Oppo et al.*, 2006] nor strong reorganisation of the AMOC [*Guihou et al.*, 2010, 2011]. Thus, similarly to the small "rebound" events at the end of GIS 21 and 23, we suggest that GIS 25 could be a response to the slow cooling phase occurring during MIS 5.5 induced by a decreasing local summer insolation. This progressive cooling can increase sea ice formation resulting in saltier surface waters [e.g., *Jochum et al.*, 2012]. At a certain point, a resumption of the AMOC can be triggered, leading to NH high-latitude warming, enhancing accumulation and ice sheet growth. Such a recovery of the AMOC may only affect the North Atlantic region. This hypothesis that calls for processes originating in the high latitudes of the NH needs further investigation involving improved synchronisations between ice cores and other paleoclimatic archives. So far, neither of these two hypotheses (muted event or regional event) can be ruled out from existing data. Still, the sequence of events revealed by our new data highlights the close interplay between orbitally-driven transitions and the progressive large-scale organization of millennial-scale variability.

[18] Finally, it would be highly valuable to confront these findings with other high-resolution paleoclimatic records in the North Atlantic and other key regions. Further investigations are needed, for instance through the use of proxies of regional sea ice and precipitation potentially available from marine records or ice core aerosol series. To our knowledge, modelling studies focused on the glacial inception have only aimed at deciphering the causes of the orbital-scale cooling. Thus, dedicated simulations with state-of-the-art climate models need to be performed under climatic conditions characteristic of the glacial inception to test whether the initiation of millennial-scale climatic variability may be triggered by locally forced mechanisms or point instead to remote regions. The present dataset obtained within one ice core and therefore unaffected by chronological problems provide a challenging benchmark for modelling the non-linear response of the Earth system to the well-known orbital forcing and an interesting case study to test the sensitivity of late interglacials to abrupt climate change.

Appendix A

[19] The δD measurements have been performed at LSCE through an automatic injection device and a technique based on uranium reduction of water to H_2 gas with an associated analytical accuracy of ± 0.5‰ at 1σ [*Vaughn et al.*, 1998]. The high resolution $\delta^{18}O_{ice}$ profile has been obtained at the Niels Bohr Institute for Astronomy (University of Copenhagen). Measurements were performed using a CO_2 equilibration technique [*Epstein*, 1953] with an analytical precision of 0.07‰. The d-excess calculation is therefore associated with a quadratic uncertainty of 0.75‰. Methane concentrations measurements were conducted at LGGE. The air from ice samples of 50 g is extracted with a melt-refreezing method under vacuum, and the extracted gas is then analysed for CH_4 by gas chromatography accompanied by a mean analytical uncertainty (1σ) of 8 ppbv [*Chappellaz et al.*, 1993].

[20] Measurements of $\delta^{15}N$ of N_2 and $\delta^{18}O$ of O_2 were carried out at LSCE. For each depth, two adjacent ice samples (10g each) covering the same depth interval were cut from the ice core. As depicted in *Sowers et al.* [1989] and *Landais et al.* [2004a, 2004b], the trapped air is extracted by melting

the samples under vacuum. The water is then refrozen and the gases remaining in the headspace are cryogenically trapped in a steel tube at liquid He temperature. The isotopic measurements are then performed on a Thermo Delta V Plus that permits simultaneous acquisition of m/z 32 and 28. Corrections are applied for pressure imbalance and chemical interference for all measurements. The $\delta^{18}O$ of paleoatmospheric O_2 ($\delta^{18}O_{atm}$) is obtained after correction for gravitational and thermal fractionation in the firn (i.e. the unconsolidated snow that constitutes the top 70 m of the ice sheet at the NorthGRIP site today) using the $\delta^{15}N$ data that are acquired simultaneously [*Landais et al.*, 2006]. The associated pooled standard deviation for $\delta^{15}N$ and $\delta^{18}O_{atm}$ is 0.006‰ and 0.030‰ respectively. The $\delta^{18}O_{atm}$ measurements and a low resolution $\delta^{15}N$ profile over DO 25 were published by *Landais et al.* [2006, 2010]. Here, we increased the resolution of the $\delta^{15}N$ record up to 110 years.

[21] **Acknowledgments.** We thank Nerilie Abram and Eric Wolff for their useful comments on an early version of this paper. This work is a contribution to the North Greenland Ice Core Project (NGRIP) directed and organized by the Department of Geophysics at the Niels Bohr Institute for Astronomy, Physics and Geophysics, University of Copenhagen. It is supported by funding agencies in Denmark (SNF), Belgium (FNRS-CFB), France (IPEV and INSU/CNRS), Germany (AWI), Iceland (RannIs), Japan (MEXT), Sweden (SPRS), Switzerland (SNF) and the USA (NSF, Office of Polar Programs). This work was supported by ANR PICC and ANR NEEM and by funding to the Past4Future project from the European Commission's 7th Framework Programme, grant 243908. This work is LSCE contribution 4823 and is Past4Future contribution 23.

[22] The Editor thanks two anonymous reviewers for assisting in the evaluation of this paper.

References

Berger, A. (1988), Milankovitch theory and climate, *Rev. Geophys.*, *26*, 624–657, doi:10.1029/RG026i004p00624.

Bintanja, R., et al. (2005), Modelled atmospheric temperatures and global sea levels over the past million years, *Nature*, *437*, 125–128, doi:10.1038/nature03975.

Broecker, W. S. (1998), Paleocean circulation during the last deglaciation: A bipolar seesaw?, *Paleoceanography*, *13*, 119–121, doi:10.1029/97PA03707.

Brook, E. J., et al. (1996), Rapid variations in atmospheric methane concentration during the past 110000 years, *Science*, *273*, 1087–1091, doi:10.1126/science.273.5278.1087.

Caballero-Gill, R. P., S. Clemens, and W. Prell (2012), Antarctic Isotope Maxima events 24 and 25 identified in benthic marine $\delta^{18}O$, *Paleoceanography*, *27*, PA1101, doi:10.1029/2011PA002269.

Cane, M. (1998), A role for the tropical Pacific, *Science*, *282*, 59–61, doi:10.1126/science.282.5386.59.

Capron, E., et al. (2010a), Millennial and sub-millennial scale climatic variations recorded in polar ice cores over the last glacial period, *Clim. Past*, *6*, 345–365, doi:10.5194/cp-6-345-2010.

Capron, E., et al. (2010b), Synchronising EDML and NorthGRIP ice cores using $\delta^{18}O$ of atmospheric oxygen ($\delta^{18}O_{atm}$) and CH_4 measurements over MIS 5 (80–123 kyr), *Quat. Sci. Rev.*, *29*, 222–234, doi:10.1016/j.quascirev.2009.07.014.

Chapman, M. R., and N. J. Shackleton (1999), Global ice-volume fluctuations, North Atlantic ice-rafted events, and deep-ocean circulation changes between 130 and 70 ka, *Geology*, *27*, 795–798, doi:10.1130/0091-7613(1999)027<0795:GIVFNA>2.3.CO;2.

Chappellaz, J., et al. (1993), Synchronous changes in atmospheric CH_4 and Greenland climate between 40 kyr and 8 kyr BP, *Nature*, *366*, 443–445, doi:10.1038/366443a0.

Chiang, J. C. H., and C. M. Bitz (2005), The influence of high latitude ice cover on the marine Intertropical Convergence Zone, *Clim. Dyn.*, *25*, 477–496, doi:10.1007/s00382-005-0040-5.

Dansgaard, W. (1964), Stable isotopes in precipitation, *Tellus, Ser. A*, *16*, 436–468, doi:10.1111/j.2153-3490.1964.tb00181.x.

Denton, G. H., et al. (2005), The role of seasonality in abrupt climate change, *Quat. Sci. Rev.*, *24*, 1159–1182, doi:10.1016/j.quascirev.2004.12.002.

EPICA Community Members (2006), One-to-one coupling of glacial climate variability in Greenland and Antarctica, *Nature*, *444*, 195–198, doi:10.1038/nature05301.

Epstein, S. (1953), Revised carbonate-water isotopic temperature scale, *Geol. Soc. Am. Bull.*, *64*, 1315–1326, doi:10.1130/0016-7606(1953)64[1315:RCITS]2.0.CO;2.

Flückiger, J., T. Blunier, B. Stauffer, J. Chappellaz, R. Spahni, K. Kawamura, J. Schwander, T. F. Stocker, and D. Dahl-Jensen (2004), N_2O and CH_4 variations during the last glacial epoch: Insight into global processes, *Global Biogeochem. Cycles*, *18*, GB1020, doi:10.1029/2003GB002122.

Fuchs, A., and M. C. Leuenberger (1996), $\delta^{18}O$ of atmospheric oxygen measured on the GRIP Ice Core Document Stratigraphic disturbances in the lowest 10% of the core, *Geophys. Res. Lett.*, *23*(9), 1049–1052, doi:10.1029/96GL00588.

Goujon, C., J.-M. Barnola, and C. Ritz (2003), Modeling the densification of polar firn including heat diffusion: Application to close-off characteristics and gas isotopic fractionation for Antarctica and Greenland sites, *J. Geophys. Res.*, *108*(D24), 4792, doi:10.1029/2002JD003319.

Guihou, A., et al. (2010), Late slowdown of the Atlantic meridional overturning circulation during the last glacial inception: New constraints from sedimentary ($^{231}Pa/^{230}Th$), *Earth Planet. Sci. Lett.*, *289*, 520–529, doi:10.1016/j.epsl.2009.11.045.

Guihou, A., et al. (2011), Enhanced Atlantic meridional overturning circulation supports the last glacial inception, *Quat. Sci. Rev.*, *30*, 1576–1582, doi:10.1016/j.quascirev.2011.03.017.

Huber, C., et al. (2006), Isotope calibrated Greenland temperature record over Marine Isotope Stage 3 and its relation to CH_4, *Earth Planet. Sci. Lett.*, *243*, 504–519, doi:10.1016/j.epsl.2006.01.002.

Jochum, M., et al. (2012), True to Milankovitch: Glacial inception in the new Community Climate System Model, *J. Clim.*, *25*, 2226–2239, doi:10.1175/JCLI-D-11-00044.1.

Johnsen, S. J. et al. (2000), Diffusion of stable isotopes in polar firn and ice: The isotope effect in firn diffusion, in *Physics of Ice Core Records*, edited by T. Hondoh, pp. 121–140, Hokkaido Univ. Press, Sapporo, Japan.

Jouzel, J., et al. (2007), Orbital and millennial Antarctic climate variability over the past 800,000 years, *Science*, *317*, 793–796, doi:10.1126/science.1141038.

Kageyama, M., et al. (2010), Modelling glacial climatic millennial-scale variability related to changes in the Atlantic meridional overturning circulation: A review, *Quat. Sci. Rev.*, *29*, 2931–2956, doi:10.1016/j.quascirev.2010.05.029.

Khodri, M., et al. (2001), Simulating the amplification of orbital forcing by ocean feedbacks in the last glaciations, *Nature*, *410*, 570–574, doi:10.1038/35069044.

Knorr, G., and G. Lohmann (2003), Southern Ocean origin for the resumption of Atlantic thermohaline during deglaciation, *Nature*, *424*, 532–536, doi:10.1038/nature01855.

Landais, A., et al. (2004a), Quantification of rapid temperature change during DO event 12 and phasing with methane inferred from air isotopic measurements, *Earth Planet. Sci. Lett.*, *225*, 221–232, doi:10.1016/j.epsl.2004.06.009.

Landais, A., J. P. Steffensen, N. Caillon, J. Jouzel, V. Masson-Delmotte, and J. Schwander (2004b), Evidence for stratigraphic distortion in the Greenland Ice Core Project (GRIP) ice core during Event 5e1 (120 kyr BP) from gas isotopes, *J. Geophys. Res.*, *109*, D06103, doi:10.1029/2003JD004193.

Landais, A., et al. (2006), The glacial inception as recorded in the NorthGRIP Greenland ice core: Timing, structure and associated abrupt temperature changes, *Clim. Dyn.*, *26*, 273–284, doi:10.1007/s00382-005-0063-y.

Landais, A., et al. (2010), What drives orbital- and millennial-scale variations of the $\delta^{18}O$ of atmospheric oxygen?, *Quat. Sci. Rev.*, *29*, 235–246, doi:10.1016/j.quascirev.2009.07.005.

Laskar, J., et al. (2004), A long-term numerical solution for the insolation quantities of the Earth, *Astron. Astrophys.*, *428*, 261–285, doi:10.1051/0004-6361:20041335.

Lüthi, D., et al. (2008), High-resolution carbon dioxide concentration record 650,000–800,000 years before present, *Nature*, *453*, 379–382, doi:10.1038/nature06949.

Masson-Delmotte, V., et al. (2005), Deuterium excess reveals millennial and orbital scale fluctuations of Greenland moisture origin, *Science*, *309*, 118–121, doi:10.1126/science.1108575.

McManus, J. F., et al. (2002), Thermohaline circulation and prolonged interglacial warmth in the North Atlantic, *Quat. Res.*, *58*, 17–21, doi:10.1006/qres.2002.2367.

Mudelsee, M. (2000), Ramp function regression: A tool for quantifying climate transitions, *Comput. Geosci.*, *26*, 293–307, doi:10.1016/S0098-3004(99)00141-7.

NorthGRIP Community Members (2004), High-resolution record of Northern Hemisphere climate extending into the last interglacial period, *Nature*, *431*, 147–151, doi:10.1038/nature02805.

Oppo, D., et al. (2006), Evolution and demise of the last interglacial warmth in the subpolar North Atlantic, *Quat. Sci. Rev.*, *25*, 3268–3277, doi:10.1016/j.quascirev.2006.07.006.

Parrenin, F., et al. (2007), The EDC3 chronology for the EDC ice core, *Clim. Past*, *3*, 485–497, doi:10.5194/cp-3-485-2007.

Sanchez-Goñi, M. F., et al. (2002), Synchroneity between marine and terrestrial responses to millennial scale climatic variability during the last glacial period in the Mediterranean region, *Clim. Dyn.*, *19*, 95–105, doi:10.1007/s00382-001-0212-x.

Severinghaus, J., et al. (1998), Timing of abrupt climate change at the end of the Younger Dryas interval from thermally fractionated gases in polar ice, *Nature*, *391*, 141–146, doi:10.1038/34346.

Severinghaus, J., et al. (2009), Oxygen-18 of O_2 records the impact of abrupt climate change on the terrestrial biosphere, *Science*, *324*, 1431–1434, doi:10.1126/science.1169473.

Sowers, T., M. Bender, and D. Raynaud (1989), Elemental and isotopic composition of occluded O_2 and N_2 in polar ice, *J. Geophys. Res.*, *94*(D4), 5137–5150, doi:10.1029/JD094iD04p05137.

Spahni, R., J. Schwander, J. Flückiger, B. Stauffer, J. Chappellaz, and D. Raynaud (2003), The attenuation of fast atmospheric CH_4 variations recorded in polar ice cores, *Geophys. Res. Lett.*, *30*(11), 1571, doi:10.1029/2003GL017093.

Stenni, B., et al. (2010), The deuterium excess records of EPICA Dome C and Dronning Maud Land ice cores (East Antarctica), *Quat. Sci. Rev.*, *29*, 146–159, doi:10.1016/j.quascirev.2009.10.009.

Stocker, T. F. (2000), Past and future reorganisations in the climate system, *Quat. Sci. Rev.*, *19*, 301–319.

Stocker, T. F., and S. J. Johnsen (2003), A minimum thermodynamic model for the bipolar seesaw, *Paleoceanography*, *18*(4), 1087, doi:10.1029/2003PA000920.

Thompson, W. G., and S. I. Goldstein (2005), Open-system coral ages reveal persistent sub-orbital sea level cycles, *Science*, *308*, 401–404, doi:10.1126/science.1104035.

Tziperman, E., M. E. Raymo, P. Huybers, and C. Wunsch (2006), Consequences of pacing the Pleistocene 100 kyr ice ages by nonlinear phase locking to Milankovitch forcing, *Paleoceanography*, *21*, PA4206, doi:10.1029/2005PA001241.

Vaughn, B., et al. (1998), An automated system for the uranium reduction method of hydrogen isotope analysis of water, *Chem. Geol.*, *152*, 309–319, doi:10.1016/S0009-2541(98)00117-X.

Voelker, A. H. L., et al. (2002), Global distribution of centennial-scale records for Marine Isotope Stage (MIS) 3: A database, *Quat. Sci. Rev.*, *21*, 1185–1212, doi:10.1016/S0277-3791(01)00139-1.

Wang, Z., and L. A. Mysak (2002), Simulation of the last glacial inception and rapid ice sheet growth in the McGill Paleoclimate Model, *Geophys. Res. Lett.*, *29*(23), 2102, doi:10.1029/2002GL015120.

Wang, Y., et al. (2008), Millennial- and orbital-scale changes in the East Asian monsoon over the past 224,000 years, *Nature*, *451*, 1090–1093, doi:10.1038/nature06692.